Biosensors and Bioelectronics 126 (2019) 792–799

Contents lists available at ScienceDirect

Biosensors and Bioelectronics

journal homepage: www.elsevier.com/locate/bios

A smart nanosensor for the detection of human immunodeficiency virus and associated cardiovascular and arthritis diseases using functionalized graphene-based transistors

Saurav Islam[a,1], Shruti Shukla[c], Vivek K. Bajpai[c], Young-Kyu Han[c,*], Yun Suk Huh[d,*], Ashok Kumar[e], Arindam Ghosh[a,b], Sonu Gandhi[f,*,1]

[a] Department of Physics, Indian Institute of Science (IISc), Bangalore 560012, India
[b] Center for Nanoscience and Engineering, Indian Institute of Science (IISc), Bangalore 560012, India
[c] Department of Energy and Materials Engineering, Dongguk University, 30 Pildongro 1-gil, Seoul 04620, Republic of Korea
[d] Department of Biological Engineering, Biohybrid Systems Research Center (BSRC), Inha University, 100 Inha-ro, Nam-gu, Incheon 22212, Republic of Korea
[e] CSIR-Institute of Genomics and Integrative Biology (CSIR-IGIB), Mall Road, New Delhi 110007, India
[f] DBT-National Institute of Animal Biotechnology (DBT-NIAB), Hyderabad 500032, Telangana, India

ARTICLE INFO

Keywords:
Biosensor
Graphene
Immunoassay
Transistor
HIV
Cardiac troponin 1
Rheumatoid arthritis

ABSTRACT

Human immunodeficiency virus (HIV), which isa worldwide public health issue, is commonly associated with cardiovascular disorders (CVDs) and rheumatoid arthritis (RA). A smart nanosensor was developed for the detection of HIV and its related diseases (CVDs and RA) using graphene-based field-effect transistors (FETs). In this study, amine-functionalized graphene (afG) was conjugated with antibodies [anti-p24 for HIV, anti-cardiac troponin 1 (anti-cTn1) for CVDs, and anti-cyclic citrullinated peptide (anti-CCP) for RA] to detect various biomarkers. The antibodies were covalently conjugated to afG via carbodiimide activation. The bioconjugate (graphene-antibody) was characterized by various biophysical techniques such as UV–Vis, Raman spectroscopy, scanning electron microscopy (SEM), and atomic force microscopy (AFM). The electrochemical performance of the sensor was evaluated with respect to changes in the resistance of the electrode surface due to the interaction of the antigen with its specific antibody. The developed sensor was highly sensitive and showed a linear response to p24, cTn1, and, CCP from 1 fg/mL to 1 μg/mL. The limit of detection (LOD) was 100 fg/mL for p24 and 10 fg/mL for cTn1 and CCP under standard optimized conditions. The graphene-based smart nanodevice demonstrated excellent performance; thus, it could be used for the on-site detection of HIV, CVD, and RA biomarkers in real samples.

1. Introduction

Human immunodeficiency virus (HIV) has transformed into a global epidemic and emerged as a multisystem disorder, primarily involving the cardiovascular and musculoskeletal system (Lipshultz et al., 1989; Nanavati et al., 2004; Winchester et al., 1987). HIV-induced drug interactions or manifestations that cause cardiovascular disorders (CVDs) in HIV patients are the leading causes of morbidity and mortality. The HIV-CVD association often remains clinically undiagnosed or wrongly attributed to other non-cardiac diseases such as chronic obstructive pulmonary disease (COPD) and obstructive sleep apnea (OSA) (Ferreira et al., 2015).

Increased awareness and routine screening for cardiovascular symptoms in HIV patients can aid in early diagnosis and contribute to a better treatment regimen. Various observational cohort studies have been carried out, the results of which showed an increased risk in acute myocardial infarction among HIV-infected patients compared with control individuals (Currier et al., 2003; Durand et al., 2011; Triant et al., 2007). Moreover, a systematic review and meta-analysis conducted by Islam et al. (2012), with the aim to estimate the risk of CVDs for HIV-infected patients compared with healthy individuals, found that HIV infection could increase the risk of CVDs by 61%. Some HIV-associated CVDs include infective endocarditis (Rerkpattanapipat et al., 2000), pulmonary hypertension (Almodovar et al., 2011), pericardial effusion (Eisenberg et al., 1992), and premature atherosclerosis (Calza et al., 2008). HIV-associated musculoskeletal disorders have been

* Corresponding authors.
E-mail addresses: ykhan1972@gmail.com (Y.-K. Han), yunsuk.huh@inha.ac.kr (Y.S. Huh), gandhi@niab.org.in (S. Gandhi).
[1] Sonu Gandhi and Saurav Islam contributed equally to this work.

https://doi.org/10.1016/j.bios.2018.11.041
Received 27 September 2018; Received in revised form 13 November 2018; Accepted 28 November 2018
Available online 07 December 2018
0956-5663/

reported since the outbreak of this global epidemic. Patients with HIV can develop arthritis at any stage of the disease (Kaddu-Mukasa et al., 2011). Moreover, serological markers of arthritis can be found in HIV-infected patients (du Toit et al., 2011). Articular syndromes are associated with HIV, such as sero negative spondylo arthropathy (SPA) (McGonagle et al., 2001), rheumatoid arthritis (RA) (Carroll et al., 2016), and articular syndrome (Plate and Boyle, 2003), which could increase the risk of cardiovascular disease among patients with RA (Gonzalez-Juanatey et al., 2003; Nurmohamed, 2009).

A number of immunological and electrochemical assays have been developed for the detection of HIV and its associated diseases (CVDs and RA)(Biancotto et al., 2009; Fonseca et al., 2011; Hashida et al., 1998; Li et al., 2009). The diagnosis of HIV (primarily associated with the detection of p24 antigen), RA, and CVDs is mainly performed using immunological assays such as enzyme-linked immunosorbent assay, western blot assay, and immunofluorescence assay (Cho et al., 2009; Hayes et al., 2009; Ishikawa et al., 1998; Tabushi et al., 2008). Immunosensors provide a promising alternative approach for the detection of various biomolecules such as those of pesticides, narcotic drugs, cancer, pre-eclampsia, HIV, CVDs, and RA (Suri et al., 2008, 2009; Sharma et al., 2010; Thakur et al., 2011; Gandhi et al., 2008, 2009, 2015, 2016, 2018; Tey et al., 2010; Singh et al., 2018; Suman et al., 2017; Gan et al., 2013; Munje et al., 2015; Zhao et al., 2018).

Advancements in electrochemical immunosensing have allowed better detection methods to be developed with a simple design at a low cost with high selectivity, sensitivity, and field applicability (Wijaya et al., 2009, 2010; Talan et al., 2018). Moraes et al. (2014) developed electrochemical immunosensors based on the biorecognition between anti-p24 antibody and its antigenic peptide p24-3 (from HIV-1 p24 protein). The antigenic peptide was incorporated inside liposomes to build layer-by-layer films with polyethyleneimine with a limit of detection (LOD) up to 1 μg/mL. Munje et al. (2015) developed label-free, electrochemical sensors using zinc oxide (ZnO) nanowires for the detection of cardiac troponin T or cardiac troponin 1 (cTnTor cTn1). Electrochemical impedance spectroscopy (EIS) and fluorescence quantification analysis were performed to determine the linear detection range of cTnT or cTn1 in the human blood. The detection limit, which was found to be 10 fg/mL, has potential utility in point-of-care (POC) diagnostics for cardiovascular diseases. In another study, a novel, label-free, electro-generated chemiluminescence immunosensor for the early diagnosis of RA was developed with a LOD of 0.2 pg/mL using heterogeneous polyaniline-gold nanomaterial (Zhao et al., 2018). A real-time label-free assay was developed for the detection of cTn1 up to 2 ng/mL using selectively functionalized SnO_2 field-effect transistors (FETs) (Cheng et al., 2011).

Nevertheless, most of the known methods require sophisticated instrumentation and a high analytical time and may not be suitable for real-time, on-site applications. In contrast, charge sensitive sensors using two-dimensional graphene offer several key advantages, such as ultra-high sensitivity, ease of operation, and a short response time, and can be easily integrated into a chip for point-of-care testing (POCT).

In the present study, we have developed a smart FET-based nanodevice for the detection of HIV, CVD, and RA biomarkers using amine-functionalized graphene (afG) conjugated with specific antibodies. The FETs were fabricated from both single and multilayer graphene, which work at very low noise levels (Karnatak et al., 2016, 2017; Pal and Ghosh, 2009a, 2009b; Pal et al., 2011), and were obtained using the scotch tape exfoliation technique on 285 nm SiO_2/Si substrate followed by standard electron beam lithography and metallization using 5/40 nm Cr/Au.

The specific antibodies [anti-p24 for HIV, anti-cardiac troponin 1 (anti-cTn1) for CVDs, and anti-cyclic citrullinated peptide (anti-CCP) for RA] were covalently conjugated to afG via carbodiimide activation. The interaction of the target antigen, bound to the graphene surface, with it's specific antibody leads to a redistribution of the local doping, which manisfests as change in the resistance of the graphene channel, which can be used to determine the concentration of the analyte. The results demonstrate that the developed smart nanodevice could potentially be used for the rapid, on-site detection of not only HIV, CVD, and RA biomarkers but also other disease markers.

2. Material and methods

2.1. Reagents

For exfoliation, single crystals of Kish graphite purchased from the Covalent Materials Corp. (Tokyo, Japan) were used. In addition, 285 nm Si/SiO_2 substrate was purchased from Nova Electronic Materials (Flower Mound, TX, USA). For thermal evaporation, 99.99% pure gold wire and chromium pellets were obtained from Kurt J. Lesker Co. (Clairton,PA, USA). Scotch tape (3 M) was used for exfoliating graphene. PMMA 495 and 950 were obtained from MicroChem Corp. (Newton, MA, USA). 1-ethyl-3-(3-dimethylaminopropyl)carbodiimide hydrochloride (EDC) and N-hydroxysulfosuccinimide (sulfo-NHS) were purchased from Sigma-Aldrich (Delhi, India). Polyclonal antibodies and antigens (for p24, cTn1, and CCP) were purchased from Abcam (Cambridge, UK). All other reagents used were of high-quality analytical grade unless otherwise stated. All solutions were prepared using double-distilled water.

2.2. Apparatus

The UV–Vis spectrum was acquired using Analytikjena SPECORD S-600 (Noida, India) witha range of 200–1020 nm. A Raman spectrometer (Thermo-Nicolet 6700; Bangalore, India) was used to obtain Raman spectra. Fourier transform infrared (FT-IR) spectroscopy was performed using the Shimadzu 8700 FT-IR spectrophotometer (Noida, India). The synthesized bioconjugate was characterized by scanning electron microscopy (SEM)(Zeiss EVO 18 448;Noida, India). Surface morphology was examined by optical microscopy (Olympus BX51; Bangalore, India) and atomic force microscopy (AFM) (Veeco CP-II;SBK, Bangalore, India). All electrical measurements were performed using the SR 830 lock-in amplifier at a carrier frequency of 227.9 Hz. The gate voltage for obtaining the transfer characteristics was applied using Keithley 2400 Source Meter. All experiments were performed at room temperature (RT)(25 ± 1 °C).

2.3. Functionalization and labeling of graphene with antibodies

Antibody binding (for p24, cTn1, CCP) was performed via 1-ethyl-3-(3-dimethyl aminopropyl) carbodiimide hydrochloride (EDC) and N-hydroxysuccinimide (NHS) carbodiimide chemistry. Graphene (0.5 mg) was allowed to react with 75 μM EDC and 75 μM NHS (total volume 1 mL) for 2 h under gentle stirring at RT. The activated complex of graphene was centrifuged at 10,000 rpm for 15 min at 4 °C followed by the resuspension of the pellet in 1 mL phosphate buffer (PB; 50 mM,pH 7.4). The antibodies (100 μg each for p24, cTn1, and CCP) were separately added dropwise to the activated graphene for 30 min at RT followed by overnight incubation at 4 °C. The pellet (graphene-antibody) was centrifuged, resuspended in 0.5 mL PB (pH 7.4), and further characterized by spectroscopic and microscopic techniques to confirm antibody binding. Binding of antibody to nanocomplex was determined indirectly using a Bradford assay to measure protein with rabbit IgG as the standard. Briefly, the nanocomplex (0.1 μg/mL) was conjugated with different concentrations of antibody (0.1, 0.5, and 1 mg/mL) followed by centrifugation (10,000 rpm; 10 min) to remove any unbound antibodies. The washing procedure was repeated three times using 500 μL of 0.1 M phosphate buffer and the wash solution was collectively measured to determine the concentration of unbound antibodies. A standard curve of absorbance versus rabbit IgG concentration was generated by measuring the absorbance at various concentrations.

2.4. Characterization of the bioconjugate

The developed bioconjugate with all three antibodies (p24, cTn1, and CCP) was characterized separately by various microscopic and spectroscopic techniques such as SEM, AFM, UV–Vis, FT-IR, and Raman spectroscopy. The obtained spectra of graphene and the graphene-antibody bioconjugate were compared. SEM was performed to confirm the labeling of graphene with the respective antibodies. The UV–Vis absorption spectra of the afG-antibody bioconjugate were obtained in the range of 200–500 nm. Raman spectra were acquired in the range of 1300–3000 cm^{-1} to examine the change in the characteristics of graphene before and after antibody labeling. FT-IR was performed in the range of 500–4000 cm^{-1}.

2.5. Fabrication of FETs

To fabricate the FETs, graphene was first exfoliated from a single crystal of graphite using the scotch tape technique on 285 nm SiO_2/Si substrate with SiO_2 as the back-gate dielectric. Suitable graphene flakes, both single and multi-layers, were identified witha high-resolution optical microscope (Olympus BX 51;Bangalore, India) at 200–1000 × magnification in reflection mode after exfoliation. The substrates were then coated with one layer each of PMMA 495 and PMMA 950, which formed the positive resist for electron beam lithography (Raith Pioneer;Bangalore, India). After lithography, the samples were developed in a solution of isopropyl alcohol (IPA) and methyl isobutyl ketone (MIBK) with a ratio of 3:1, followed by the thermal evaporation of Cr and Au (thickness of 5 nm and 50 nm, respectively), which formed the source-drain contacts. The samples were then mounted on a ceramic chip carrier and ball-bonded using a TPT wirebonder.

2.6. Electrochemical characterization of the developed nanodevice

The antibodies (p24, cTn1,and CCP) were immobilized separately on the surface of the FET, pre-activated with EDC/NHS, and allowed to bind with graphene for 30 min. Following antibody addition, the antibodies were immobilized with 50 mM PB (pH 7.4). PB washes were performed at each step to remove excess and unbound material. Blocking was performed with 1% BSA in 50 mM PB (pH 7.4), and the

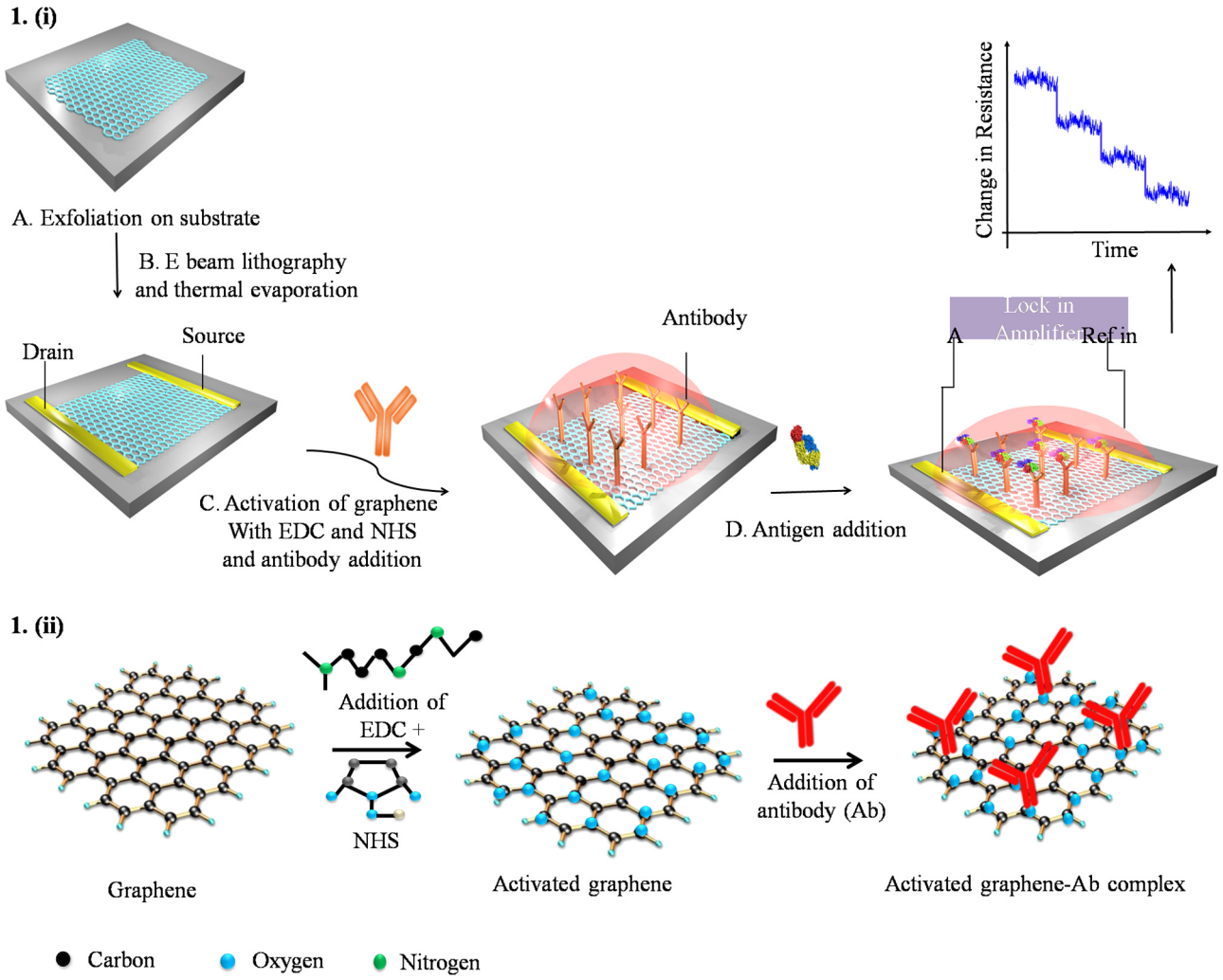

Scheme 1. (i) Fabrication of the graphene immunosensor. (A) Graphene was first exfoliated on 285 nm SiO_2/Si substrate with SiO_2 as the back-gate dielectric. (B) After exfoliation, the source-drain contact pads were defined by electron beam lithography, followed by the thermal evaporation of 5/50 nm Cr/Au. (C) After the fabrication of the field-effect transistor (FET), graphene was functionalized with antibodies by drop-casting them on the graphene channel, and non-specific sites were blocked by a blocking agent. (D) Biosensing was performed by adding specific antigens to the functionalized graphene. The resistance of the graphene channel was monitored continuously using a lock-in amplifier with various antigen concentrations, which could give a quantitative estimate of the detection capabilities of the graphene biosensor. **(ii)** Activation procedure for antibody (Ab) conjugation to the graphene nanomaterial using the carbodiimide method. 1-Ethyl-3-(3-dimethylaminopropyl)carbodiimide hydrochloride (EDC) and N-hydroxysulfosuccinimide (NHS) were used for the activation of carboxylic groups on the surface of graphene, enhancing the formation of activated graphene-antibody complexes via amino groups.

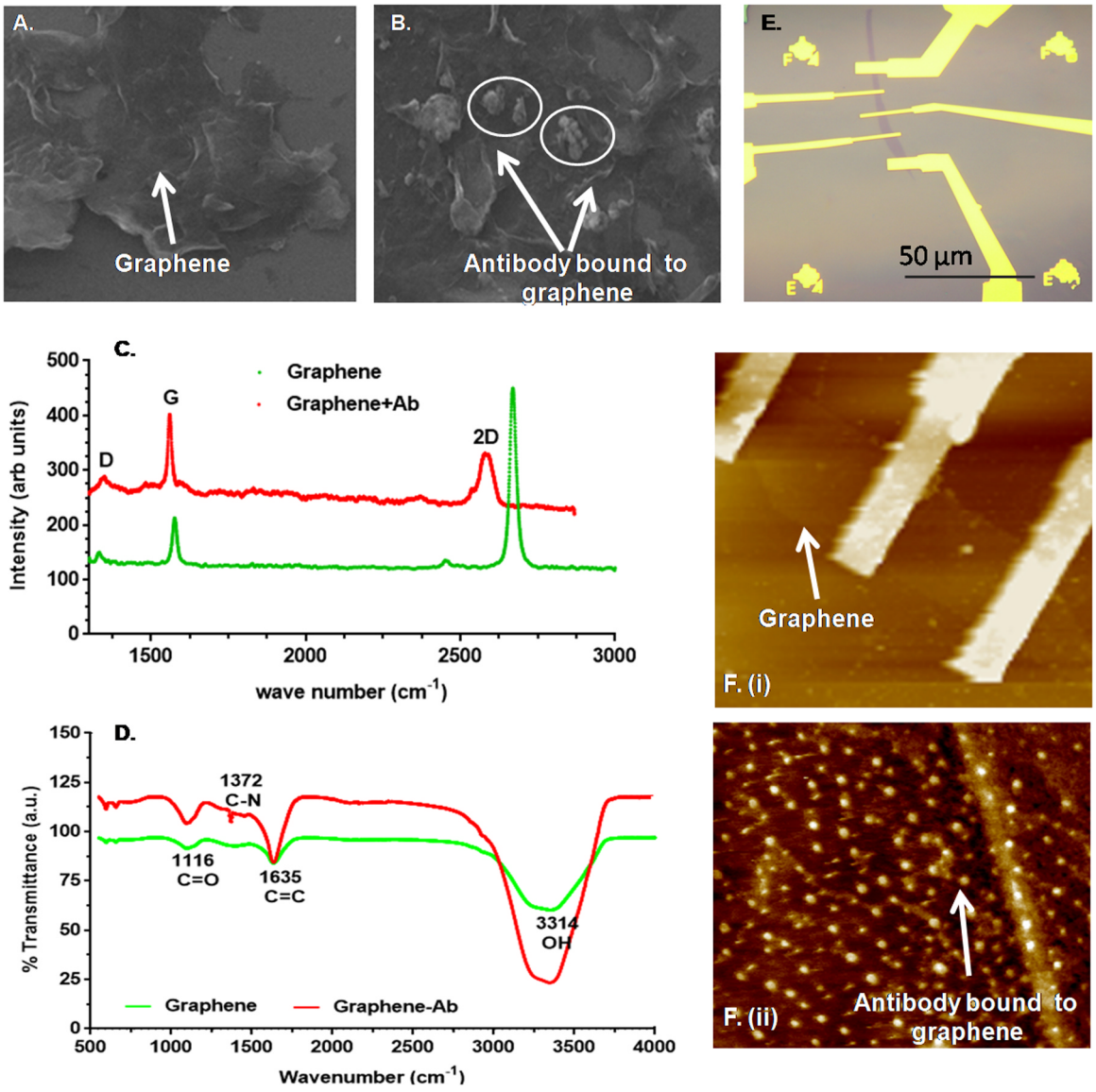

Fig. 1. Characterization of antibody-labeled graphene. (A) Scanning electron microscopy (SEM) analysis of the surface morphology of graphene showed that graphene was clearly visible. (B) SEM analysis of the graphene-antibody bioconjugate revealed a white proteinaceous material on the surface of graphene, indicating antibody binding. (C) Optical micrograph of a typical graphene field-effect transistor (FET) before measurement. (D) (i) AFM image showed the bare graphene without antibody binding; (ii) The brighter spots in Atomic force microscopy (AFM) indicated antibody-antigen binding on the graphene surface. (E) Raman spectra confirmed antibody bindingon the graphene surface. (F) Fourier transform infrared (FT-IR) peaks were found at 1116 and 1635 cm^{-1} for C=O and C-C, respectively.

device was used for analyte detection. Antigen concentrations were prepared in the range of 1 fg/mL to 1 µg/mL (in 50 mM PB; pH 7.4) separately for electrochemical sensing. Liquid state measurements were performed,and the change in the resistance was recorded at different stages using a constant current circuit by passing 100 nA of current through the FET. The reproducibility of the graphene-based FET immunosensor was evaluated with three different electrodes by adding antigens (p24, cTn1, and CCP) at fixed concentrations and monitoring the resistance. Furthermore, cross-reactivity analysis was performed to determine the specificity of the developed device for p24, cTn1, and CCP.

3. Results and discussion

3.1. Characterization and confirmation of antibody-labeled graphene (bioconjugate)

Scheme 1 shows the bioconjugation of antibodies with graphene. Surface morphology analysis was performed by SEM to confirm the labeling of graphene with antibodies (p24, cTn1, and CCP). Graphene was clearly visible as shown in Fig. 1A. In the case of the graphene-antibody bioconjugate, a white proteinaceous material (indicating bounded antibodies) was observed on the surface of graphene as shown in Fig. 1B. UV–Vis spectra (Fig. S1) revealed are the shift of 5 nm with a peak at 230 nm for graphene (green line) and at 235 nm for graphene-antibody (red line). Similarly, the Raman spectra in Fig. 1C demonstrated antibody binding. In Fig. 1D, the FT-IR spectra revealed peaks at 1116 and 1635 cm^{-1} for C=O and C-C, respectively. The peak at 1372 cm^{-1} for C-N confirmed the binding between graphene and the antibodies (Saleem et al., 2016; Yang et al., 2009). Table S1 showed the binding affinity of antibody with graphene nanocomplex prior to antigen reaction. As the enhanced binding efficiency will be directly concerned with increased antigen-antibody reaction. The affinity of antibodies against specific antigens (HIV, cTn1, and RA) in the presence of graphene before immobilization on the surface of FET is upto 90% at 1 mg/mL antibody concentration.

3.2. Electrochemical characterization of the developed graphene-based FETs

Scheme 1 shows the fabrication process of the FET device with graphene and immobilization of antibodies on its surface via carbodiimide activation. Fig. 1E shows the optical image of a typical graphene FET fabricated using the exfoliation method. The morphological characteristics of the graphene FET device shows the presence of antibodies (p24, cTn1, and CCP) on the graphene FET surface. The AFM image of bare graphene in Fig. 1F (i) and F(ii) confirmed the presence of antibodies (white dots) with a change of 5 nm in the height profile, which confirmed the binding of the antibodies to the graphene surface (Yuri et al., 2014).

3.3. Analytical performance of the developed FET nanodevice for detecting HIV, CVD, and RA biomarkers

The first step in fabricating the biosensor was to functionalize the graphene channel with antibodies. Antibodies were drop-casted on the carboxylated graphene FET, which bound to its surface by covalent bonding and π-π interactions (Kuila et al., 2011). Each biosensor had two parts (the receptor and the transducer). Here, the antibodies act as specific sites for the antigens to bind and form the receptor, whereas the graphene layer acts as the transducer, which converts a chemical signal from antibody-antigen interactions into a readable electrical signal (Shao et al., 2010; Pumera, 2011; Waqas et al., 2016).

The resistance vs. gate voltage (V_g) of the graphene FET demonstrated ambipolar behavior with a charge neutrality point at −1 V (Fig. S1B), 8 V (Figs. S1C), and −1 V (Fig. S1D),-, indicating different intrinsic doping levels in these devices. The change in the intrinsic doping profile of graphene was determined based on the change in the position of the Dirac point before and after the measurement cycle as demonstrated in Fig. 2A. The change in the charge neutrality point voltage was ΔV_{CNP}~8V. The resultant doping of graphene can be calculated with $\Delta ne = C\Delta V_{CNP}$, where Δn is the change in the carrier number of graphene, e is the electronic charge, ΔV_{CNP} is the change in the Dirac point of the graphene channel before and after measurements., and $C = 1.2\times10^{-4}$ F is the capacitance of 285 nm SiO_2. The change in number density was calculated as 6.0×10^{15} m^{-2} for cTn1 antibodies, thus confirming the binding between the graphene channel and the biomolecules. For further confirmation of antibody binding on the graphene surface, 0.01 μg/mL of antibodies were drop-casted directly on a gold FET device (Fig. 2B). The absence of measurable changes confirmed that the signal originated from antibodies bound with graphene (Fig. S1D). For field applicability, the stability of the device functionalized with antibodies was monitored up to three weeks. The graphene FET device was stored at RT, and the resistance was monitored from time to time. The device characteristics were stable for four weeks with a negligible change in the resistance (Fig. 2C).

To quantify the response of the graphene conjugated with specific biomarkers (as a biomolecule sensor), the antigens were drop-cast on multiple graphene-based FETs, and kinetic measurements were performed (Fig. 3). Antibody-antigen interactions led to a change in the doping profile of the graphene channel with a change in the resistance, which was monitored continuously at $V_g = 0$ V for HIV antigen concentrations ranging from 1 fg/mL to 1 μg/mL. The response was linear as shown in Fig. 3B. For a more quantitative understanding of the biosensing capabilities of the sensors, the percentage change in channel resistance was calculated by taking the resistance in the buffer solution as the baseline. The change was almost 21% for an antigen concentration of 1 μg/mL, beyond which it showed saturation (Fig. 3). This may be attributed to the utilization of all active sites; thus, the further addition of antibodies would not lead to additional binding due to the absence of active sites. The limit of detection for HIV antibodies with different detection methods is shown in Fig. S2A (Nakatsuma et al., 2015). The limit of detection for HIV using functionalized graphene was 100 fg/mL, making it one of the most sensitive detectors available for HIV antigens (Table 1). As the electrical response to the added antigens was almost instantaneous, the analytical time of the device was extremely short.

Using a similar technique, we also investigated the sensing capabilities of graphene for cTn1(CVD) and CCP (rheumatic arthritis) antibodies, which are diseases associated with HIV, by monitoring the resistance change for analyte concentrations ranging from 1 fg/mL to 1 μg/mL. The response of the device as a function of antigen concentration for cTn1 and CCP is shown in Fig. 3C and E, respectively. The percentage change in the resistance is shown in Fig. 3D and E. The

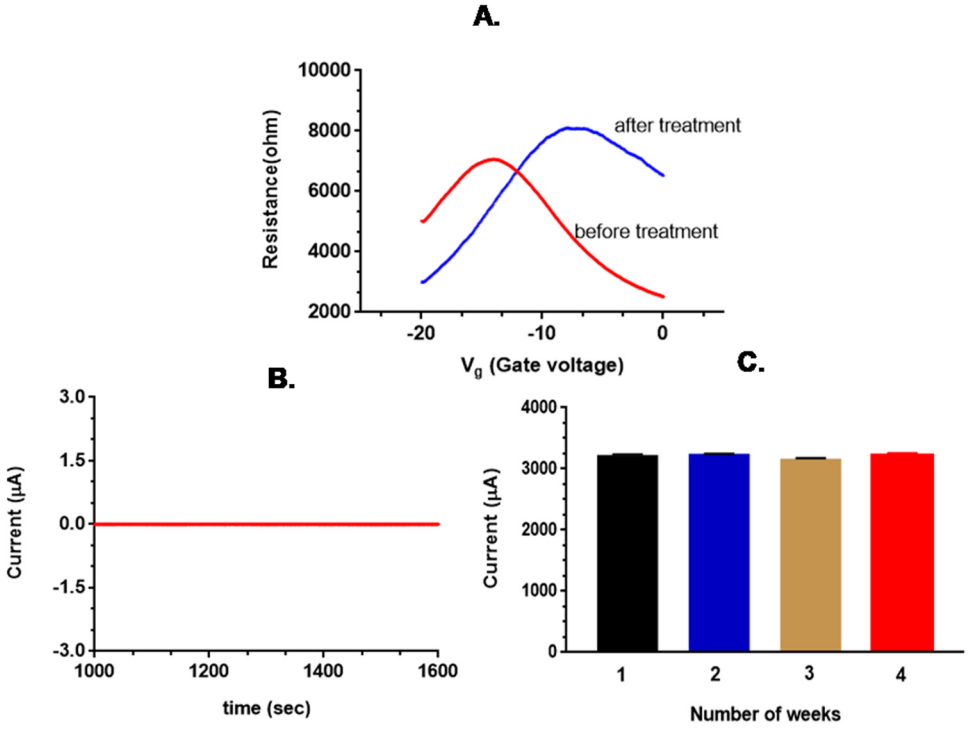

Fig. 2. (A) The current vs. time plot of the graphene field-effect transistor (FET) monitored over four weeks. The negligible change in the current demonstrated the stability of the devices. (B) The current response on the gold surface indicated no antibody binding, thus demonstrating the role of graphene in binding. (C) Device measurements performed before (-15 mV) and after (-5 mV) treatment with antibodies revealed a significant change in the gate voltage (V_g).

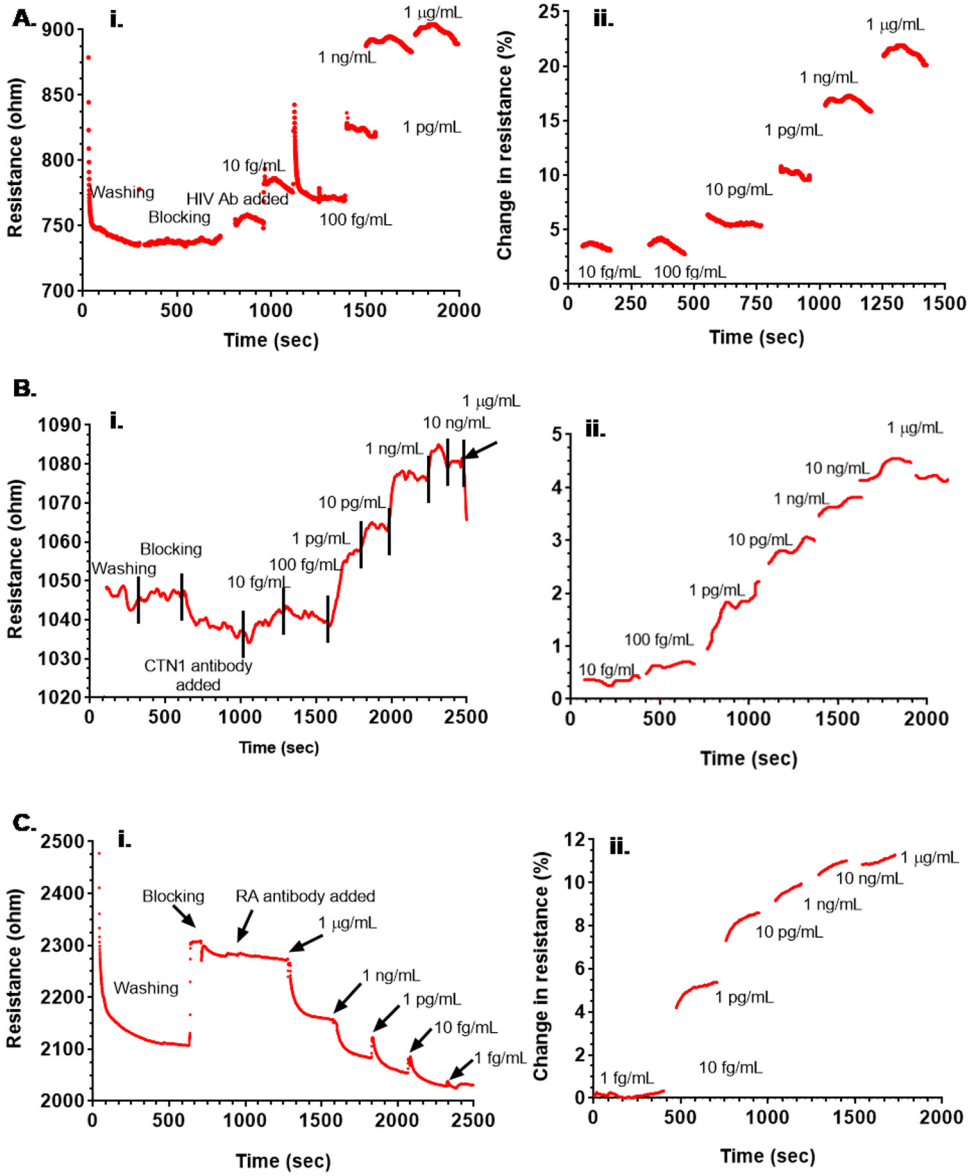

Fig. 3. Kinetic response of the graphene biosensor at various concentrations of antigens for (A-i) p24, (B-i) cTn1, and (C-i) CCP. Percentage change in the resistance of the biosensor at different concentrations of antigens for p24, cTn1, and CCP (A-ii, B-ii, and C-ii, respectively). The device showed a linear response from 1fg/mL to 1 µg/mL with a limit of detection (LOD) of 100 fg/mL.

graphene channel demonstrated an excellent response in both cases with a linear range from 1 fg/mL to 1 µg/mL. The LOD for cTn1 and RA was 10 fg/mL, which is one of the highest (Fig. S2B) reported in the literature thus far (Table 1). As shown in Fig. 4, the developed device exhibited reproducible behavior at fixed concentrations of antigens [4 A: p24 (100 fg/mL), 4B: cTn1 (10 µg/mL), 4 C: CCP (10 µg/mL)]. Cross-reactivity analysis revealed the specific nature of the graphene FET device fabricated with specific antibodies, which did not show any cross-reactivity to non-specific antigens as shown in Fig. 4 [4E(i&ii): p24, 4F(i&ii): cTn1, 4 G(i&ii): CCP]. The detection method using the functionalized graphene FET outperformed most other known methods (calorimetric, fluorescence, or electrochemical) for cTn1 detection in key parameters such as the LOD and analytical time (Ha et al., 2016a, 2016b).

4. Conclusion

Our study has revealed that graphene can be an extremely sensitive

Table 1
Comparison of various electrochemical immunosensors based on field effect transistors (FETs) with its linear range, and limit of detection.

Name of the disease and associated biomarkers	Nanomaterial	Linear range	Limit of detection (LOD)	Reference
Myocardial infarction (cTn1)	SnO_2 nanowire	–	2 ng/mL	Cheng et al. (2011)
Acute myocardial infarction (cTn1)	Silicon nanowire	0.092– 46 ng/mL	0.092 ng/mL	Kong et al. (2012)
Cardiac disease (cTn1)	Silicon nanowire	5 pg/mL–5 ng/mL	5 pg/mL	Kim et al. (2016)
HIV	Graphene	1 p.M. to 10 nM	1 p.M.	Kwon et al. (2013)
HIV, cTn1, RA	Graphene	1 fg/mL to 1 µg/mL	100 fg/mL (HIV); 10 fg/mL (cTn1, and CCP)	Present work

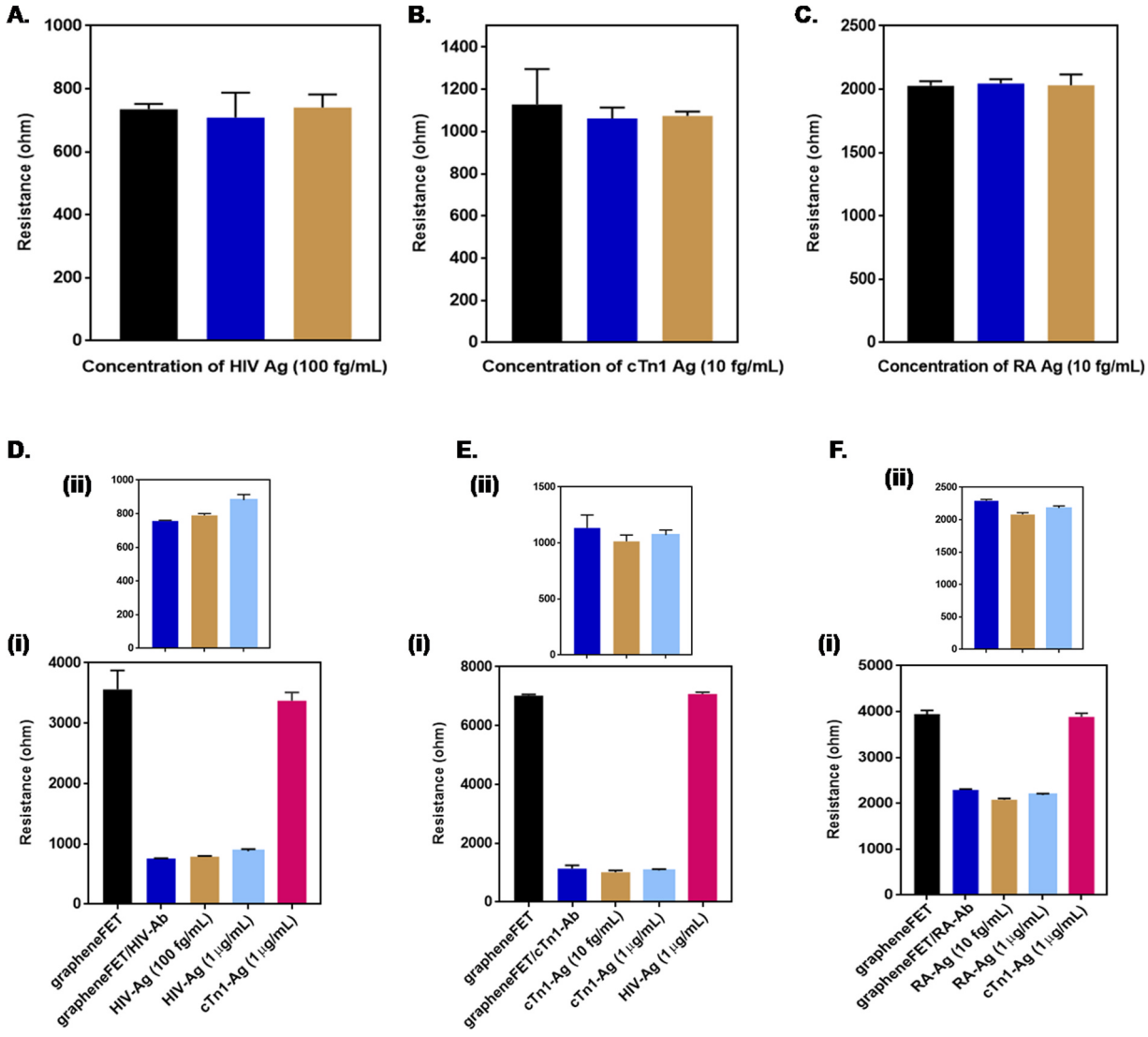

Fig. 4. Reproducibility studies of fabricated graphene FET immunosensor at fixed concentration of antigen (A- HIV; B- cTn1; C- RA). The resistance was measured on the three individual graFET sensor. Cross-reactivity experiments were performed for three different antigen (D-i- HIV; E-i- cTn1; F-i- RA); inset shows the enlarged view of the same as in case of (D-ii- HIV; E-ii- cTn1; F-ii- RA).

platform for the detection of HIV and related cardiovascular diseases and arthritis. The developed sensor was highly sensitive and showed a linear response to p24, cTn1, and, CCP from 1 fg/mL to 1 µg/mL with a LOD of 100 fg/mL for p24 and 10 fg/mL for cTn1 and CCP under standard conditions. The detection technique of the developed graphene-based FET immunosensor exhibited a clear advantage over conventional techniques because of its quick response time and increased selectivity and sensitivity. Therefore, the graphene-based smart nanodevice demonstrated excellent performance with a high POCT potential for the on-site detection of HIV, CVD, and RA biomarkers in real samples. However, the miniaturization of the device for field applicability would be costly/expensive. We are currently pursuing the development of a cost-effective graphene-based sensor by using alternate fabrication procedures, which could be used as a diagnostic platform to detect potential disease markers.

Acknowledgement

Sonu Gandhi*, Saurav Islam* contributed equally to this work. S.G. conceived the idea. S.G. and S.I. performed, analysed the experimental results and wrote the manuscript. S. S., V. K. B., Y.K. H., Y. S. H., A. K., A. G. authors helped in the discussion and revision of the manuscript. The authors are grateful to Department of Biotechnology (DBT-Biocare), New Delhi, Grant number (BT/PR18069/BIC/101/574/2016) for supporting this research and Tokyo Electron Limited, Tokyo, Japan.

Appendix A. Supplementary material

Supplementary data associated with this article can be found in the online version at doi:10.1016/j.bios.2018.11.041.

References

Almodovar, S., Hsue, P.Y., Morelli, J., Huang, L., Flores, S.C., 2011. Proc. Am. Thorac. Soc. 8, 308–312.
Biancotto, A., Brichacek, B., Chen, S.S., Fitzgerald, W., Lisco, A., Vanpouille, C., Margolis, L., Grivel, J.C., 2009. J. Virol. Methods 157, 98–101.
Calza, L., Manfredi, R., Pocaterra, D., Chiodo, F., 2008. J. Infect. 57, 16–32.
Carroll, M.B., Fields, J.H., Clerc, P.G., 2016. Open Access Rheumatol. 8, 51–59.
Cheng, Y., Chen, K.S., Meyer, N.L., Yuan, J., Hirst, L.S., Chase, P.B., Xiong, P., 2011. Biosens. Bioelectron. 26, 4538–4544.
Cho, I.H., Paek, E.H., Kim, Y.K., Kim, J.H., Paek, S.H., 2009. Anal. Chim. Acta 632, 247–255.
Currier, J.S., Taylor, A., Boyd, F., Dezii, C.M., Kawabata, H., Burtcel, B., Maa, J.F., Hodder, S., 2003. J. Acquir. Immune Defic. Syndr. 33, 506–512.
du Toit, R., Whitelaw, D., Taljaard, J.J., du Plessis, L., Esser, M., 2011. J. Rheumatol. 38, 1055–1060.

Durand, M., Sheehy, O., Baril, J.G., Lelorier, J., Tremblay, C.L., 2011. J. Acquir. Immune Defic. Syndr. 57, 245–253.
Eisenberg, M.J., Gordon, A.S., Schiller, N.B., 1992. Chest 102, 956–958.
Ferreira, C., Providência, R., Ferreira, M.J., Gonçalves, L.M., 2015. Arq. Bras. Cardiol. 105, 519–526.
Fonseca, R.A.S., Ramos-Jesus, J., Kubota, L.T., Dutra, R.F., 2011. Sensors 11, 10785–10797.
Gan, N., Du, X., Cao, Y., Hu, F., Li, T., Qianli, J., 2013. Materials 6, 1255–1269.
Gandhi, S., Sharma, P., Capalash, N., Verma, R.S., Suri, C.R., 2008. Anal. Bioanal. Chem. 392, 215–222.
Gandhi, S., Capalash, N., Sharma, P., Suri, C.R., 2009. Biosens. Bioelectron. 25, 502–505.
Gandhi, S., Suman, P., Kumar, A., Sharma, P., Capalash, N., Suri, C.R., 2015. BioImpacts 5, 207–213.
Gandhi, S., Arami, H., Krishnan, K.M., 2016. Nanolett 16, 3668–3674.
Gandhi, S., Banga, I., Maurya, P.K., Eremin, S.A., 2018. RSC Adv. 8, 1511–1518.
Gonzalez-Juanatey, C., Llorca, J., Testa, A., Revuelta, J., Garcia-Porrua, C., Gonzalez-Gay, M.A., 2003. Medicine 82, 407–413.
Ha, X., Li, S., Peng, Z., Othman, A.M., Leblanc, R., 2016a. ACS Sens. 1, 106–114.
Hashida, S., Ishikawa, S., Hashinaka, K., Nishikata, I., Saito, A., Takamizawa, A., Shinagawa, H., Ishikawa, E., 1998. J. Clin. Lab. Anal. 12, 115–120.
Hayes, M.A., Petkus, M.M., Garcia, A.A., Taylor, T., Mahanti, P., 2009. Analyst 134, 533–541.
Ishikawa, E., Ishikawa, S., Hashida, S., Hashinaka, K., 1998. J. Clin. Lab. Anal. 12, 154–161.
Islam, F.M., Wu, J., Jansson, J., Wilson, D.P., 2012. HIV Med. 13, 453–468.
Kaddu-Mukasa, M., Ssekasanvu, E., Ddumba, E., Thomas, D., Katabira, E.T., 2011. Afr. Health Sci. 11, 24–29.
Karnatak, P., Sai, T.P., Goswami, S., Ghatak, S., Kaushal, S., Ghosh, A., 2016. Nat. Commun. 7, 13703.
Karnatak, P., Paul, T., Islam, S., Ghosh, A., 2017. Adv. Phy: X. 2, 428–449.
Kim, K., Park, C., Kwon, D., Kim, D., Meyyappan, M., Jeon, S., Lee, J.S., 2016. Biosens. Bioelectron. 77, 695–701.
Kong, T., Su, R., Zhang, B., Zhang, Q., Cheng, G., 2012. Biosens. Bioelectron. 34, 267–272.
Kuila, T., Bose, S., Khanra, P., Mishra, A.K., Kim, N.H., Lee, J.H., 2011. Biosens. Bioelectron. 26, 4637–4648.
Kwon, O.S., Lee, S.H., Park, S.J., An, J.H., Song, H.S., Kim, T., Oh, J.H., Bae, J., Yoon, H., Park, T.H., Jang, J., 2013. Adv. Mater. 25, 4177–4185.
Li, J., Xie, W., Fang, N., Yeung, E.S., 2009. Anal. Bioanal. Chem. 394, 489–497.
Lipshultz, S.E., Chanock, S., Sanders, S.P., Perez-Atayde, A., McIntosh, K., 1989. Am. J. Cardiol. 63, 1489–1497.
McGonagle, D., Reade, S., Ortega, H., Gibbon, W., O'Connor, P., Morgan, A., Melsom, R., Morgan, E., Emery, P., 2001. Ann. Rheum. Dis. 60, 696–698.
Moraes, M., Rodrigues, V., Soares, J., Ferreira, M., de Souza, N., Oliveira, O., 2014. J. Nanosci. Nanotechnol. 14, 1–8.
Munje, R.D., Jacobs, M., Muthukumar, S., Quadri, B., Shanmugam, N.R., Prasad, S., 2015. Anal. Methods 7, 10136–10144.
Nanavati, K.A., Fisher, S.D., Miller, T.L., Lipshultz, S.E., 2004. Am. J. Cardiovasc. Drugs 4, 315–324.
Nakatsuma, A., Kaneda, M., Kodama, H., Morikawa, M., Watabe, S., Nakaishi, K., Yamashita, M., Yoshimura, T., Miura, T., Ninomiya, M., 2015. PLoS One 10, e0131319.
Nurmohamed, M.T., 2009. Autoimmun. Rev. 8, 663–667.
Pal, A.N., Ghosh, A., 2009a. Phys. Rev. Lett. 102, 126805.
Pal, A.N., Ghosh, A., 2009b. Appl. Phys. Lett. 95, 082105.
Pal, A.N., Ghatak, S., Kochat, V., Sneha, E.S., Sampathkumar, A., Raghavan, S., Ghosh, A., 2011. ACS Nano. 5, 2075–2081.
Plate, A.M., Boyle, B.A., 2003. AIDS Read. 13, 69–70.
Pumera, M., 2011. Mat. Today 14, 308–315.
Rerkpattanapipat, P., Wongpraparut, N., Jacobs, L.E., Kotler, M.N., 2000. Arch. Intern. Med. 160, 602–608.
Sharma, P., Gandhi, S., Suri, C.R., 2010. Anal. Chim. Acta 676, 87–92.
Shao, Y., Wang, J., Wu, H., Liu, J., Aksay, I.A., Lina, Y., 2010. Electroanal 22, 1027–1036.
Ha, X., Li, S., PengZ, Othman, M.A., Leblanc, R., 2016b. ACS Sens. 1, 106–114.
Singh, S., Mishra, P., Banga, I., Parmar, A.S., Tripathi, P.P., Gandhi, S., 2018. Bioimpacts 8, 57–62.
Suman, P., Gandhi, S., Kumar, P., Garg, K., 2017. Am. J. Reprod. Immunol. 77, 1–10.
Suri, C.R., Kaur, J., Gandhi, S., Shekhawat, G.S., 2008. J. Nanotechnol. 19, 235502.
Suri, C.R., Boro, R., Nangia, Y., Gandhi, S., Wangoo, N., Sharma, P., Shekhawat, G.S., 2009. Trends Anal. Chem. 28, 29–31.
Tabushi, Y., Nakanishi, T., Takeuchi, T., Nakajima, M., Ueda, K., Kotani, T., Makino, S., Shimizu, A., Hanafusa, T., Takubo, T., 2008. Ann. Clin. Biochem. 45, 413–417.
Talan, A., Mishra, A., Eremin, S.A., Narang, J., Kumar, A., Gandhi, S., 2018. Biosens. Bioelectron. 105, 14–21.
Tey, J.N., Gandhi, S., Wijaya, I.P.M., Palaniappan, Al, Wei, J., Rodriguez, I., Suri, C.R., Mhaisalkar, S.G., 2010. Small 6, 993–998.
Thakur, S., Gandhi, S., Paul, A.K., Suri, C.R., 2011. Sens. Trans. 131, 91–100.
Triant, V.A., Lee, H., Hadigan, C., Grinspoon, S.K., 2007. J. Clin. Endocrinol. Metab. 92, 2506–2512.
Waqas, S., Carlos, S., Brian, W., Gavin, G., Sharma, A.C., Ghosh, R., 2016. Biosens. Bioelectron. 86, 522–529.
Wijaya, I.P.M., Gandhi, S., Tey, J.N., Wangoo, N., Shekhawat, G.S., Suri, C.R., Rodriguez, I., Mhaisalkar, S.G., 2009. Appl. Phys. Lett. 95, 073704.
Wijaya, I.P.M., Tey, J.N., Gandhi, S., Boro, R., Rodriguez, I., Mhaisalkar, S.G., Suri, C.R., Palaniappan, Al, Hau, G.W., 2010. Lab Chip. 10, 634–638.
Winchester, R., Bernstein, D., Fischer, H., Enlow, R., Solomon, G., 1987. Ann. Intern. Med. 106, 19–26.
Yang, H.F., Li, F.H., Shan, C.S., Han, D.X., Zhang, Q.X., Niu, L., Ivaska, 2009. A. J. Mat. Chem. 19, 4632–4638.
Yuri, D.I., Natalia, S.B., Tatyana, O.P., Pavel, A.F., Elena, Y.A., Anna, L.K., Victor, G.Z., Alexander, A.I., Tatyana, I.P., Vadim, S.Z., Sergey, P.R., Sergei, A.M., Alexander, I.A., 2014. Int. J. Nanomed. 9, 4659–4670.
Zhao, Y., Liu, Y., Li, X., Wang, H., Zhang, Y., Ma, H., Wei, Q., 2018. Sens. Actuators B Chem. 257, 354–361.